Formation and Characterization of Semiflexible Polymer Networks via Monte Carlo Simulations

Dhananjay M. Bhawe, Claude Cohen, and Fernando A. Escobedo*

School of Chemical and Biomolecular Engineering, Cornell University, Ithaca, New York 14853

Received October 2, 2003; Revised Manuscript Received March 9, 2004

ABSTRACT: The effect of chain stiffness and entanglements on deformation properties of end-linked networks was investigated using Monte Carlo simulations. Tetrafunctionally cross-linked monodisperse networks were prepared in the framework of the bond fluctuation model (BFM). The degree of entanglement in these networks was tuned by changing the initial polymer concentration at curing (Φ_0). The chain stiffness was controlled by using an adjustable bond angle bending potential. Continuum-space simulations of isotropic swelling and uniaxial deformation were carried out in isobaric and isostress ensembles, respectively. Both equilibrium swelling and stress−strain data indicate that the stiffer chain networks are more entangled, confirming previous simulation results on polymer melts. For such entangled networks, stiffer chains are associated with a higher elastic modulus and smaller equilibrium swelling; the opposite is true, however, for entanglement-free "diamond" networks. The elastic modulus determined from low-strain uniaxial deformations agrees with semitheoretical predictions for moderate chain stiffness, but not for very stiff chains. For the realistically cross-linked (and hence entangled) networks studied here, the theoretically predicted strain-induced discontinuous ordering transition was not observed, although the transition region becomes narrower for the least entangled networks made from the stiffest chains. Entanglement-free diamond networks do exhibit a discontinuous transition from a disordered state to a nematic-like state under uniaxial extension.

1. Introduction

The elastic and swelling properties of isotropic polymer networks have been extensively studied using theory[1−14] and, to a lesser extent, by simulations.[15−25] The earliest theories like the affine[1,2] and phantom[3,4] models accounted only for the entropy changes in network chains on deformation and were somewhat successful in describing qualitatively the behavior of real networks at small strains. More complex theories account for trapped entanglements by restricting cross-link motion[5−9] or by restricting chain motion by constraints along the chain contour.[10−14] However, polymer networks are inherently complex systems, and no current theory can satisfactorily explain all aspects of their behavior. Recently, there has been interest in networks made from semirigid or less flexible chains due to their potential applications as stress−optical switches, strain temperature devices, and membranes with regulated permeability.[26] These systems are even more complicated than the ordinary networks, and there is a limited amount of theoretical studies.[27−31] Warner et al.[30,31] studied nematic elastomers using a nematic mean-field type of interaction, while Mark et al.[27−29] used a more realistic approach that includes semiflexible chains with excluded-volume interactions. The main prediction of these studies is an order−disorder transition under strain. Mark et al.'s study[27−29] (which is more closely related to our simulated systems) predicts a phase transition to an ordered state upon uniaxial extension. (One of the possible conditions for such a transition is when their stiffness parameter, x, is approximately 5 or greater for a chain length of 20 Kuhn segments at a strain of 500%.) A phase transition is indeed observed[32] in experiments involving poly(diethylsiloxane) (PDES) elastomers where an aligned mesomorphic state appears as a neck on uniaxial extension. However, it has been shown that the neck contains conformationally disordered crystalline domains surrounded by an amorphous matrix rather than the nematic liquid crystalline structure predicted by the above theory. Liquid crystalline elastomers also show an isotropic−nematic transition under strain.[33]

Molecular simulations can, to some extent, overcome the drawbacks of theories by explicitly incorporating relevant details of the network structure and by making available both the macroscopic deformation properties and the conformational properties of network chains. Kremer et al. used molecular dynamics (MD) to calculate the elastic modulus of end-linked polymer networks using a Rouse mode analysis in the undeformed state[15,16] and by monitoring the network relaxation after a small deformation.[17,18] Kenkare et al.[19] used discontinuous MD to study network properties like chain configurations, mean-square displacements of segments, and the elastic modulus (by Rouse mode analysis). Hölzl et al. found[20] significant nonaffine deformation behavior by using an on-lattice model. Everaers used idealized diamond lattice networks in MD simulations to isolate the effect of entanglements on the local dynamics and elastic properties of cross-linked polymer melts.[21] There have been some recent simulations of the swelling of athermal gels with explicit solvent.[22−24] Chen et al.[25] recently implemented a new hybrid lattice-continuum method to prepare and deform end-linked networks and used it to study the effect of entanglements on the elastic behavior of flexible chain networks.

There have also been some simulation studies on the phase behavior of un-cross-linked stiff-chain macromolecules.[34−37] It has been found that an isotropic−nematic transition is seen only if the density, chain stiffness, and chain length are all greater than some threshold values. To the best of our knowledge, no simulation study has

* Corresponding author. E-mail: fe13@cornell.edu.

10.1021/ma0354896 CCC: $27.50
Published on Web 04/20/2004

been carried out to investigate the behavior of stiff-chain macromolecules in a cross-linked network form.

The goal of this work is to investigate the effect of the chain stiffness and the degree of entanglements on the elastic properties of end-linked networks. The strain induced order−disorder transition in PDES described earlier is not seen in poly(dimethylsiloxane) (PDMS), which is chemically very similar. One of the factors that distinguishes PDES from PDMS is an increased chain stiffness (as seen from persistence length measurements for these polymers[38] and explained by the presence of bulkier side groups on the PDES backbone). This simulation study can shed light on the extent to which chain stiffness is responsible for the unusual behavior of PDES. Also of interest is the effect of entanglements because stiffer chains have been predicted to be more entangled in a MD simulation study[39] and in several theoretical models (e.g., see ref 40). In such models, the entanglement length N_e for long chains of N segments is found to scale with the end-to-end distance R_{ee} as $N_e \propto R_{ee}^{-\zeta}$, where ζ is a positive number. For chains of equal N, this relation predicts a lower N_e (i.e., more entanglements per chain) as stiffness and R_{ee} increase (though the predicted scaling is not applicable to our relatively short-chain systems). This dependence of entanglements on chain stiffness can be explained by viewing the entanglements as interactions between chains that strongly hinder molecular motion and conformational changes. Increasing chain stiffness leads to a decrease in local conformational mobility and to more extended configurations relative to flexible chains; these two effects could enhance both the strength and the extent of such motion-hindering interactions. (Of course, a different physical picture would arise for extreme stiffness.) Because some of the entanglements are trapped upon chain cross-linking, they are expected to have a significant effect on the properties of semiflexible chain networks.

We varied two "design" parameters in our simulated systems: chain stiffness and the precursor chain concentration. Chain stiffness was tuned by employing an adjustable bond-angle bending potential. Precursor concentration was set by changing the volume of the simulation box while keeping the number of chains fixed. This concentration was maintained constant during the cross-linking process and allowed us to control the extent of trapped entanglements in the system. The precursor chain length was fixed, and the cross-linking "times" were adjusted such that structural differences between the many networks prepared are minimized. By comparing networks with the same amount of elastic material, we were able to isolate the effect of chain stiffness and entanglements on network behavior. The simulated networks were prepared on a lattice using the bond fluctuation model (BFM)[41,42] with Monte Carlo moves that mimic diffusive dynamics. Simulations of network swelling and uniaxial extension were carried out in a continuum using the isobaric (constant NPT) and isostress (constant $NP_zP_{xy}T$) ensembles, respectively. We would like to emphasize that our networks have realistic architectures, and the simulation methods for network formation and deformation closely mimic the corresponding experiments.

Our results support previous simulation data[39] showing that stiffer chains contain more entanglements; as a result, our stiffer chain networks tend to be "tougher", i.e., they exhibit a larger elastic modulus. However, we also find that completely removing the entanglements (by using a network with a perfectly tetrafunctional chain connectivity) actually renders the stiffer-chain networks "weaker" than the corresponding flexible-chain networks. Upon uniaxial stretching, we find that trapped entanglements cause a broadening of the order−disorder transition region in the stress domain, thereby opposing the occurrence of a first-order transition. Entanglement-free model networks of stiff chains do undergo a discontinuous strain-induced transition to a nematic phase.

In the following section we describe the hybrid method of Chen et al.[25] and the modifications needed for our systems. In the section after that we present and discuss our results for swelling and for small and large uniaxial deformations. In the last section we summarize our main conclusions.

2. Simulation Methodology

2.1. Preparation of Sample Networks. We used the three-dimensional lattice BFM to prepare our sample networks of athermal 50-mer chains. Periodic boundaries in all three directions were used to reduce system size effects and to eliminate interfacial effects. All systems have 142 chains and 78 tetrafunctional cross-links, so that the stoichiometric ratio of cross-link sites to precursor polymer chain ends is $r = 1.1$. This ratio has been shown to be the optimal ratio that minimizes topological defects for fully flexible chain networks in a previous simulation study.[43] We have adopted the same value of r for our semiflexible chain networks, as the optimal values are not known for such systems. The networks are formed at three different concentrations $\Phi_0 = 1.0$, 0.5, and 0.25, where Φ_0 is defined as the volume fraction:

$$\Phi_0 = \phi_0/\phi_{melt} \tag{1}$$

where $\phi = 8\nu N_t/V$ is the fraction of occupied volume in the lattice, $N_t = nN + C$ is the total number of sites in the system, N (=50) is the number of monomers per precursor chain, n (=142) is the number of precursor chains, C (=78) is the number of cross-links, ν is the volume of a lattice site, V is the lattice volume, and 8 is the number of lattice sites occupied per mer. ϕ_0 is the value of ϕ at the actual conditions of network formation, and ϕ_{melt} is the value of ϕ at melt conditions ($\approx$0.46) in the BFM.[42] Systems with $\Phi_0 < 1$ then correspond to solution conditions where $1 - \Phi_0$ is the solvent volume fraction. We confirmed that even the lowest Φ_0 adopted here is greater than Φ^*, the volume fraction at the overlap concentration (see Table 1).

We introduced chain stiffness using a bending potential of the form[36,44]

$$E_b = k_b(1 + \cos\psi) \tag{2}$$

where k_b is an adjustable bending parameter (in units of k_BT, where k_B = Boltzmann constant and T = temperature) and ψ is the bond angle formed by three consecutive monomers on a chain. This potential energetically penalizes the smaller bond angles, and the severity of the penalty varies with k_b. A value of $k_b = 0$ corresponds to fully flexible chains while $k_b = 5$ corresponds to very stiff chains. We can relate k_b and the

Table 1. Various Properties of the Networks Used in the Deformation Studies[a]

k_b	Φ_0	N_L	N_P	N_{X2}	w_{sol}	N_{elast}	R_g^2	R_{ee}^2	ψ_{avg}	Φ^*	N_e
0	1.0	2	6	7	0	127	81.4(0.7)	487(15)	98.2	0.283	32
2	1.0	2	5	8	0	127	166(3)	1023(22)	127.4	0.097	13
	0.5	0	6	9	0	127	183(6)	1147(63)	128.0		
	0.25	1	10	4	0	127	195(2)	1228(25)	128.8		
5	1.0	0	4	11	0	127	269(2)	1786(18)	147.3	0.047	6
	0.5	1	6	8	0	127	384(4)	2605(48)	148.1		
	0.25	1	8	6	0	127	402(4)	2767(58)	148.5		

[a] N_L is the number of single chain loops, N_P is the number of pendent chains, N_{X2} is the number of cross-links having two connections, w_{sol} is the soluble fraction, N_{elast} is the number of elastic chains [$N_{elast} = \{(1 - w_{sol})n - N_L - N_P - N_{X2}\}$], R_g and R_{ee} are the radii of gyration and end-to-end distances from the BFM systems with the terms in parentheses showing the uncertainty in the values, ψ_{avg} is the average bond angle for the BFM systems, Φ^* is the overlap volume fraction as calculated from R_g^2 at $\Phi_0 = 1$ (note that all systems are far from the dilute regime), and N_e is the entanglement length for continuum melts. These N_e values[39] correspond to a slightly different chain model than the one considered in this work and thus not exactly transferable; however, they are expected to be very good estimates for our systems.

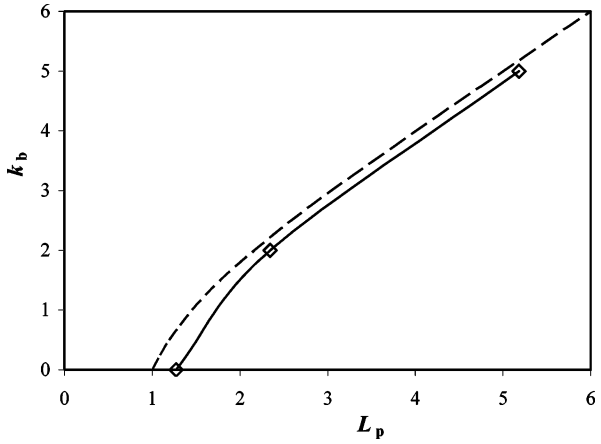

Figure 1. Chain stiffness parameter k_b (reduced by k_BT) vs the resulting persistence length L_p (reduced by the bond length b) as determined from simulations at meltlike densities (symbols) and for an ideal semiflexible chain (dashed line).

persistence length L_p by[44]

$$L_p = b/(1 + \langle \cos \psi \rangle) \tag{3}$$

where b is the average bond length and $\langle\ \rangle$ denotes an ensemble average for a system with a given k_b. For an ideal chain with no excluded-volume interactions, $\langle \cos \psi \rangle$ can be found analytically from $\langle \cos \psi \rangle = \int_0^\pi \cos \psi \exp(-E_b)\, d(\cos \psi) / \int_0^\pi \exp(-E_b)\, d(\cos \psi)$. The curves of k_b/k_BT vs L_p/b from simulation (of the continuum model described in section 2.2) and for the ideal chain are presented in Figure 1. By knowing the persistence lengths[38] of polymer species, one can determine k_b values that correspond to those species. For example, assuming that PDMS chains are fully flexible, $k_b = 0$, and from Figure 1 we get $L_{p-PDMS}/b = 1.26$; since we know[38] that $L_{p-PDES}/L_{p-PDMS} = 1.256$, it follows then that $L_{p-PDES}/b = 1.26 \times 1.256 = 1.59$, and from Figure 1 we get $k_b \approx 1$ for PDES. In this study, we have used k_b values of 0, 2, and 5.

The first step in network formation is the insertion of all the chains and cross-linkers into the simulation box. This system is then equilibrated at the desired volume fraction by using monomer and cross-linker hop moves. Afterward, curing is done by forming bonds when an unsaturated chain end and a cross-linker move into neighboring positions. The cure process is stopped when a negligible soluble fraction (<0.5%) and a large percentage of elastic material (>90%) are obtained. We varied the length of the cure simulations in such a way that all the systems prepared had the same number of elastic chains (=127). To compare our results with those of entanglement-free systems, we have used "diamond" networks in some of our simulations. A diamond network is an entanglement-free idealization of a tetrafunctional network in which all cross-links are saturated, and they would lie at the nodes of a diamond lattice when all the chains are fully stretched.

It should be noted that the Monte Carlo method adopted for network cross-linking (with its purely local moves) is known to mimic diffusive motion and produce results for dynamic behavior that are fully consistent with those from molecular dynamic simulations.[20,43]

2.2. Network Deformation. Here, we used a continuum-space network model to allow for changes in the box volume and box side lengths to proceed in a continuous manner. The chain monomers and the cross-linkers were modeled as beads of uniform diameter σ_{LJ}. The bond length b was allowed to fluctuate within a range: $\sigma_{LJ} - \Delta b \le b \le \sigma_{LJ} + \Delta b$ where $\Delta b = 0.2\sigma_{LJ}$; this is done to take into account the coarse-grained nature of the monomers and to facilitate the motion of multifunctional sites. Nonbonded beads interact via a purely repulsive Lennard-Jones (LJ) potential:

$$U_{LJ}(r) = \begin{cases} \infty & r \le r_0 \\ 4\epsilon\left\{\left(\frac{\sigma_{LJ}}{r}\right)^{12} - \left(\frac{\sigma_{LJ}}{r}\right)^{6} - \left(\frac{\sigma_{LJ}}{r_c}\right)^{12} + \left(\frac{\sigma_{LJ}}{r_c}\right)^{6}\right\} & r_0 \le r \le r_c \\ 0 & r > r_c \end{cases} \tag{4}$$

where r is the distance between two beads, $r_c = 2^{1/6}\sigma_{LJ}$ (the minimum in a normal LJ potential), $r_0 = 0.85\sigma_{LJ}$ is an overlap distance, and ϵ is the LJ energy parameter which is set such that the reduced temperature, k_BT/ϵ, is unity. This repulsive molecular model takes into account excluded-volume effects, and for a swollen system, it describes a polymer network in a good "implicit" solvent because attractive interactions between the polymer and the solvent give rise to an effective repulsion among polymer beads. The same bending potential used in the BFM lattice model (i.e., eq 2) is also used here.

To bridge the gap between the lattice BFM cure method and the off-lattice deformations, we need to transform the lattice coordinates of each BFM network into continuum coordinates. The system volume is scaled by a suitable ratio so as to maintain the same polymer volume fraction in both representations. This, however, does not bring all bond lengths within the specified continuum range ($\sigma_{LJ} - \Delta b \le b \le \sigma_{LJ} + \Delta b$),

and the system is relaxed further to achieve that. The network topology and chain structure obtained by curing in the BFM lattice are preserved upon this transformation. Note also that chain statistics like the end-to-end-distance and entanglement lengths for continuum models almost identical to ours[39] and for the BFM[42] are known to be very similar.

The system relaxation is done via "hop" and "flip" moves. Hop moves are similar to those employed in the BFM. In such a move, a randomly selected bead is displaced in a random direction by a random distance. The new position is accepted if the bond length constraints are preserved, and the conventional Metropolis criterion (based on the energy change) is satisfied. These moves are effective even for the cross-linkers that are usually tri- and tetrafunctional sites. Flip moves involve random rotation of one bead around an axis passing through the centers of its two neighbors and are used exclusively for bifunctional sites. Networks are deformed using volume moves that change the dimensions of the box. Conventional volume moves[45] that rescale the center of mass positions of single molecules with box size cannot be used in the case of cross-linked networks, as the entire system is essentially one molecule. Hence, we used highly efficient cluster volume moves to deform our networks.[23] The details of these moves and evidence of their good efficiency can be found elsewhere.[25]

It is important to point out that the pseudo-dynamic MC moves we use preclude interchain crossings. The energy barriers for such chain crossings are high; in fact, the barrier for the unlikely situation when two crossing bonds are completely stretched and perpendicular to each other is infinity [given the overlap distance r_0 adopted in eq 4], and it is $O(10^2\ k_BT)$ for configurations near that. Also, no single move can just bypass the energy barriers involved in chain crossings because any successful MC move (flip, hop, or volume move) entails only a small perturbation to the original configuration (i.e., a small bead displacement).

There are essentially two properties that require the use of box deformations: swelling and stress−strain curves. In equilibrium swelling with an implicit solvent, a uniform osmotic pressure $P^* = P\sigma_{LJ}^3/\epsilon$ is applied in all three directions; in this case, the box deformations are isotropic (i.e., the box remains cubic in shape). This osmotic pressure serves here the same role as the chemical potential (μ) in a constant μPT simulation with explicit solvent and equilibrium swelling corresponds to $P^* = 0$.[25] Stress−strain curves require anisotropic uniaxial deformations. For the uniaxial deformation runs, the off-lattice samples (with adjusted bond lengths) were first equilibrated at a melt density ($\rho \approx 0.8$, where $\rho = N_t/V$ is the network bead number density and V is the simulation box volume) by performing isotropic NPT simulations. A pressure $P^* = 3.0$ was used for these simulations as it gives the desired equilibrium density of $\rho \approx 0.8$. To induce uniaxial stretching, a smaller pressure is applied in the z direction (P_z) while the pressures along the x and y directions, P_x and P_y, are kept unchanged. Uniaxial compression is achieved by increasing P_z relative to P_x and P_y. The net stress σ along the z direction is $\{(P_x + P_y)/2 - P_z\}$, and the force applied on the sample along the z direction is $f = \sigma L_x L_y$, where L_x and L_y ($= L_x$) are the x and y dimensions of the network, respectively. The strain, λ, is given by $\lambda = L_z/L_{z,0}$, where $L_{z,0}$ and L_z are the z dimensions of the network before and after deformation. The stress values reported here for σ are made dimensionless by multiplying them by σ_{LJ}^3/k_BT. It should be noted that the equilibrium Monte Carlo methods adopted here offer a substantial advantage over molecular dynamics in efficiently simulating the network properties of interest.

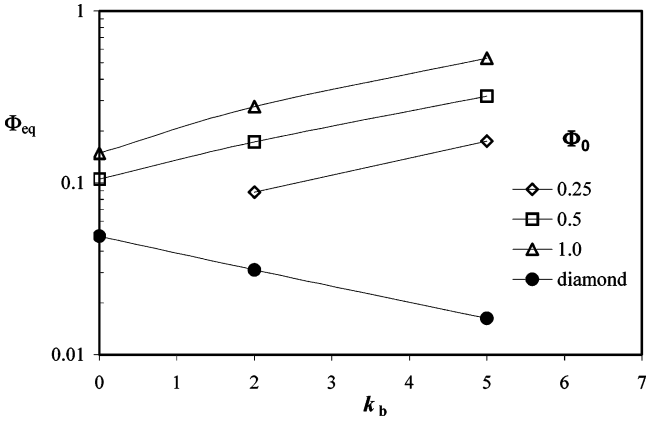

Figure 2. Equilibrium swelling volume fraction Φ_{eq} as a function of the chain stiffness k_b for various precursor volume fractions Φ_0. Also included are results for the diamond networks. The lines are drawn as guides to the eye. Error bars are commensurate to the symbols sizes.

A net orientation of chain segments along the strain axis can occur when a network is uniaxially stretched; this net alignment can be detected by the average segmental order parameter S that is calculated as

$$S = \langle P_2(\cos\theta)\rangle \tag{5}$$

where θ is the angle between the orientation of chain segments and the strain axis, P_2 is the second Legendre polynomial given by $(3\cos^2\theta - 1)/2$, and the average is over all segments. We have also analyzed the distributions of order parameter values obtained on a segmental basis and on a chain basis (i.e., averaged over all segments in individual chains).

3. Results and Discussion

The most important properties of all the networks used in this study (except the diamond networks) are listed in Table 1.

3.1. Swelling. The equilibrium swelling volume fraction Φ_{eq} for our various networks is calculated as

$$\Phi_{eq} = \rho_{eq}/\rho_{melt} \tag{6}$$

We used the bead density value from the "dry" networks for ρ_{melt} ($\approx$0.8). Figure 2 shows the simulated equilibrium swelling volume fraction as a function of the chain stiffness and the preparation volume fraction. It is observed that, at equilibrium conditions, the networks prepared at higher Φ_0 and those having stiffer chains swell less. (The volume of swollen networks is inversely proportional to Φ_{eq}.) The figure also shows the results for the diamond networks, and in this case the trend is reversed, i.e., the stiffer chain networks swell more.

As all our realistically cross-linked samples have a similar topological structure, the difference in swelling behavior can only be explained by the difference in the extent of trapped entanglements and chain stiffness. A network cured at a higher Φ_0 more readily traps entanglements than one cured at a lower Φ_0; more entanglements entail less swelling. Further, the fact that stiffer-chain networks swell less than flexible chain

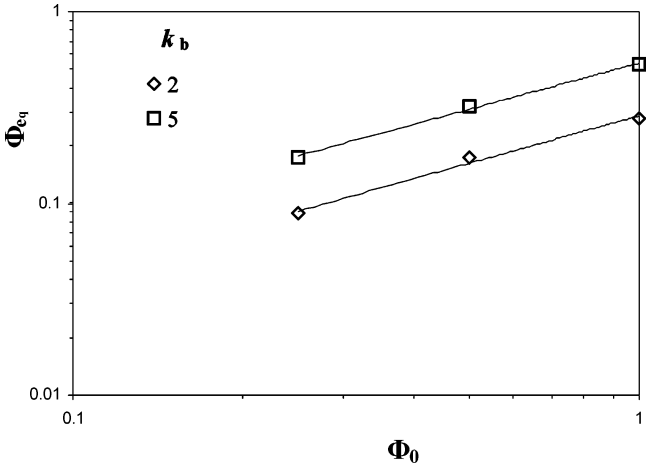

Figure 3. A log−log plot of the equilibrium swelling volume fraction (Φ_{eq}) as a function of precursor chain concentration at curing (Φ_0). The slopes of the best-fit straight lines are about 0.8 in both cases ($k_b = 2$ and 5).

networks is consistent with theoretical[40] and simulation studies[39] showing that stiffer chains are more entangled. The opposite trend observed for the diamond networks can be explained by the fact that they have no trapped entanglements. Because the solvation forces are identical irrespective of the chain stiffness, the swelling behavior solely depends on the relative change in the energy and entropy of the chains. By stretching out, the stiffer chains lose entropy, but they also reduce the bending energy by increasing the average value of the bond angle (see eq 2). The absence of trapped entanglements in the diamond networks allows the chains to readily achieve stretched conformations. This, however, is not true for the entangled networks where entanglements dominate irrespective of the cure volume fraction and restrain the chains from achieving a stretched out conformation.

The equilibrium swelling data for the entangled networks have been fitted (Figure 3) to a relation of the form $\Phi_{eq} \sim \Phi_0^{\zeta}$, yielding $\zeta \approx 0.8$ for both $k_b = 2$ and 5. It has been previously found[25] that $\zeta = 0.55$ for $k_b = 0$ (for the same chain length $N = 50$). Also, for entanglement dominated networks (i.e., where the number of entanglements per chain is far greater than the number of chemical cross-links per chain), the theoretically[46] predicted scaling exponent is $\zeta = 1.0$. These various exponent values can be explained by considering the entanglement lengths for chains of varying stiffness. These entanglement lengths can be derived by looking at the crossover from Rouse to reptation regimes of the mean-squared displacement, $g(t)$, and have been found to be $N_e = 32$, 13, and 6 for $k_b = 0$, 2, and 5, respectively.[39] This decrease in N_e with increasing k_b can be explained by the increasing radius of gyration of the chains (see Table 1). Stiffer chains span more volume in space than more flexible chains of the same contour length and therefore interact with more of their neighbor chains at a given system density. It follows from the N_e values that the networks with $k_b = 2$ and 5 are closer to being entanglement dominated (with about 4 and 8 entanglements per chain, respectively) than the fully flexible networks (1−2 entanglements per chain) and therefore yield a scaling exponent closer to 1.0. (It should be noted that several approaches exist to estimate N_e which can give different results. For fully flexible chains, Pütz et al.[47] found that N_e values from

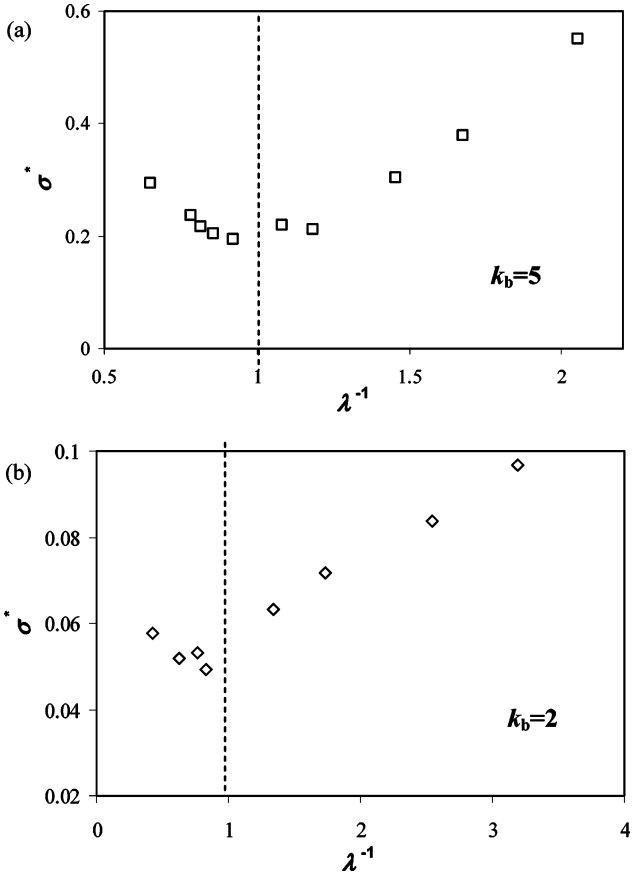

Figure 4. Mooney−Rivlin representation of uniaxial extension and compression data for networks formed at melt conditions ($\Phi_0 = 1.0$) for (a) $k_b = 5$ and (b) $k_b = 2$.

$g(t)$ were smaller than those from the stress decay on a step elongation by a factor of about 2.3. For this work, we chose to use the $g(t)$-based N_e values as no alternative estimates are available for semiflexible chains, and we are mainly interested in the relative changes of N_e with k_b.)

3.2. Low-Strain Uniaxial Deformation−Modulus Calculations. The simulated stress vs strain data are shown in Figure 4 in the Mooney−Rivlin form for $k_b = 5$ and 2 and $\Phi_0 = 1.0$, where

$$\sigma^* = \sigma/(\lambda^2 - \lambda^{-1}) \tag{7}$$

The $\lambda^{-1} > 1$ regime corresponds to uniaxial compression, and the value of σ^* at the point where the data trend intersects the $\lambda^{-1} = 1$ line corresponds to the shear modulus G (=E/3, where E is Young's modulus; values of G are in units of k_BT/σ_{LJ}^3). We obtain the following values by interpolation: $G^{(2)} \approx 0.055$ and $G^{(5)} \approx 0.18$. (The superscripts correspond to the k_b values.) A previous study[25] found $G^{(0)} \approx 0.0265$. (This value was calculated for a network with a different number of elastic chains, but it is valid here as the modulus is an intensive property and the elastic fraction is similar to that in the current study.) The net effect is that the elastic modulus increases with chain stiffness—again consistent with the prediction of increased entanglements with chain stiffness.[39,40] Other noticeable effects from Figure 4 are (i) an increase in σ^* with compression ratio, which is in contrast to a relatively flat region in the compression regime that has been observed experimentally[48] and in simulations[25] for flexible polymers, and (ii) a sharp upturn in σ^* as a function of strain that

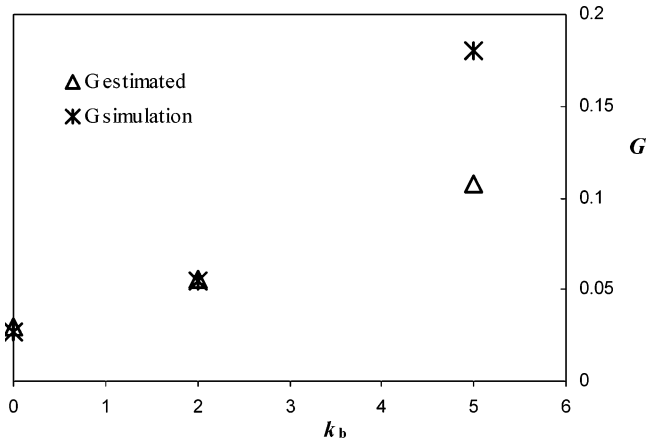

Figure 5. Comparison of simulated network elastic moduli and their semitheoretical estimates.

starts near $\lambda^{-1} = 1$ (in the extension regime); this means that the linear region is small, consistent with the highly entangled nature of these polymers.

To obtain semitheoretical estimates of the shear modulus, we divide the modulus into contributions from chemical cross-links and trapped entanglements based on the equation[49]

$$G = G_c + T_e G_e \tag{8}$$

where G_c is the cross-link contribution and G_e is the entanglement contribution. T_e is an entanglement slippage factor that may be assumed to be equal to 1.0 because the soluble fraction in our systems is negligible.[49] G_c only depends on the concentration of the cross-linkers in the system and, therefore, is the same for all values of k_b (i.e., $G_c^{(0)} = G_c^{(2)} = G_c^{(5)}$). We can therefore use the cross-link contribution obtained from the application of Rubinstein−Panyukov[50] (RP) equation to fully flexible chain networks.[25] The cross-link and entanglement contributions are, in this case, $G_c^{(0)} = 0.0115$ and $G_e^{(0)} = 0.015$. We now estimate the entanglement contribution for our semiflexible networks as

$$G_e = G_c N/N_e \tag{9}$$

Using the entanglement length values mentioned previously (see Table 1), we can estimate the shear elastic modulus for our semiflexible networks. As shown in Figure 5, these estimates match the simulated moduli well for $k_b = 0$ and 2 but not for $k_b = 5$. It should be noted that we have considered only the cross-link and entanglement contributions to the modulus (which are basically entropic in nature) while neglecting any effect from the stiffness of the chains (other than its effect on N_e). In all likelihood, the $k_b = 5$ chains are too stiff to be described by the treatment outlined above, and a more detailed theoretical study of the effect of chain stiffness (and entanglements) on network elasticity is needed.

To further elucidate the effect of entanglements, it would be instructive to simulate the shear moduli of diamond networks. However, uniaxial stretching simulations of diamond networks are difficult, especially at small strain. This is because diamond networks have no internal constraints for chain motion other than the cross-links, resulting in large fluctuations of the simulation box dimensions under a small uniaxial stress and thus very inaccurate strains. To overcome this difficulty,

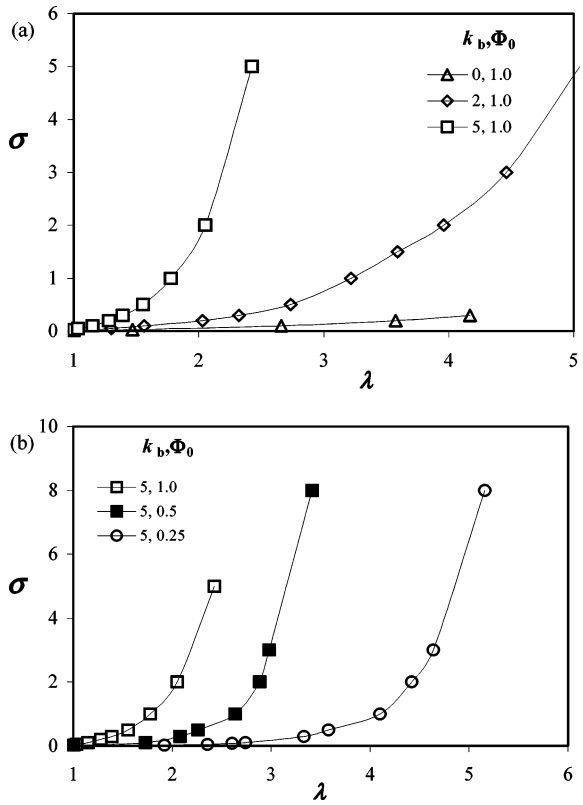

Figure 6. Stress−strain relations: (a) $\Phi_0 = 1.0$, $k_b = 0$, 2, 5; (b) $k_b = 5$, $\Phi_0 = 0.25$, 0.5, 1.0. Error bars are commensurate to twice the symbols sizes. Lines are drawn to guide the eye.

we added internal "restoring forces" to the diamond networks via a small attractive region in the interparticle potential, created by changing the potential cutoff in eq 4 from $r_c = 2^{1/6}\sigma_{LJ}$ to $1.2\sigma_{LJ}$. Such systems are now thermal (with a reduced temperature set to $k_B T/\epsilon = 0.3$) and, as such, not directly comparable to the athermal systems under consideration thus far. However, these weakly thermal diamond networks are expected to qualitatively behave like the athermal systems and to properly capture the effect of completely removing entanglements. Our preliminary modulus results[51] for $k_b = 2$ and 5 are approximately in a 2:1 ratio, which shows consistency with the swelling behavior of athermal diamond networks (shown in Figure 2); i.e., diamond networks of stiffer chains have a lower modulus than those of flexible chains.

3.3. Large-Strain Uniaxial Deformation−Measuring Order. The complete stress vs strain data for our realistically cross-linked networks are plotted in Figure 6. The cure volume fraction, Φ_0, is kept constant in Figure 6a while the stiffness, k_b, is kept constant in Figure 6b. An upturn in the stress is observed at higher values of strains, which can be associated with chains losing their configurational freedom. It is also seen that increasing stiffness causes this upturn to become sharper. Because of their greater configurational freedom, flexible chains can more readily rearrange their conformation to reduce their motion-restraining interactions with other chains; i.e., they allow entanglement "slippage" more easily than stiff chains. Also, note that stiffer chains have a less ideal (Gaussian) conformational behavior because they are shorter (in units of persistence lengths) than flexible chains; e.g., the numbers of persistence lengths (Nb/L_p) per 50-mer chain at melt conditions are ∼40, 21, and 10 for $k_b = 0$, 2, and 5,

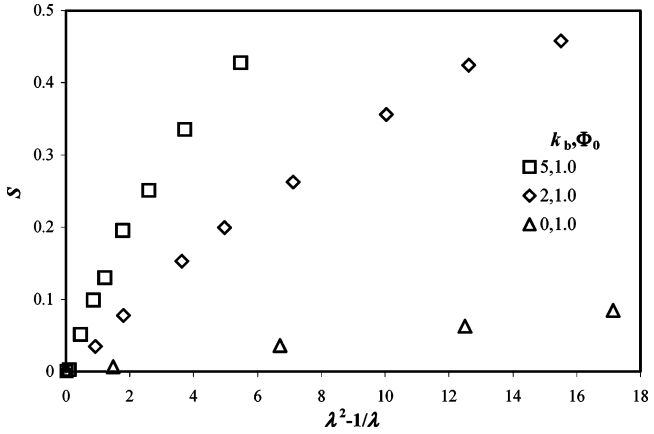

Figure 7. Segment order parameter S as a function of ($\lambda^2 - \lambda^{-1}$) for $k_b = 0$, 2, 5 and $\Phi_0 = 1.0$

respectively. This can also be seen from Table 1, where the ratio of chain end-to-end distance to radius of gyration increases from $6^{1/2}$ to almost $7^{1/2}$ as the stiffness parameter k_b increases from 0 to 5. Reducing the cure volume fraction causes the stress upturn to appear later, i.e., at a higher strain. This is because networks cured at a lower Φ_0 have less trapped entanglements and therefore more loosely coupled chains; this allows for greater strains to occur before the finite extensibility limit of some of the chains is reached.

We now examine the extent of strain-induced ordering in the networks. Figure 7 shows the segmental order parameter S (eq 5) as a function of ($\lambda^2 - \lambda^{-1}$) for a precursor volume fraction $\Phi_0 = 1$ and for $k_b = 0$, 2, and 5. In all cases, a clear increasing trend is observed for S with strain. The fact that S values for $k_b = 0$ are much smaller than those for $k_b = 2$ and 5 at the same strain indicates that chain stiffness plays a major role in promoting incipient nematic-like order ($S \geq 0.4$). Note that none of the data trends are linear as the strains involved are large and clearly not within the linear regime.

Figure 8a shows the segmental order parameter S as a function of λ for $k_b = 2$. It is seen that for equal strain the networks cured at a higher Φ_0, i.e., the more entangled systems, are more ordered; this trend was also observed by Chen et al.[25] for fully flexible chains. A similar but smaller effect is also observed for $k_b = 5$ (results not shown). For a given strain then, more entanglements seem to foster ordering on a macroscopic scale by causing the chains to interact more closely with each other; stronger interchain interactions lengthen the range of their bond-orientation correlations. Figure 8b shows the segmental order as a function of stress for $k_b = 5$. For a given stress, a more entangled network (larger Φ_0) orders significantly less (lower S), primarily because of a smaller strain. Such an effect, however, is almost absent for the $k_b = 2$ system (results not shown), which underlines the higher proclivity for ordering in the $k_b = 5$ system. In fact, it is observed that for the least entangled, stiffer-chain system (i.e., for $\Phi_0 = 0.25$ and $k_b = 5$) both strain and order increase very rapidly at rather small stresses. Had such increases been discontinuous, they would have signaled a first-order ordering transition.

The order parameter of a stretched network reaches the approximate nematic threshold value of $S \approx 0.5$ for a system-dependent value of the stress σ_{nem}. Because $S = 0$ for $\sigma = 0$, a larger value of σ_{nem} can be associated

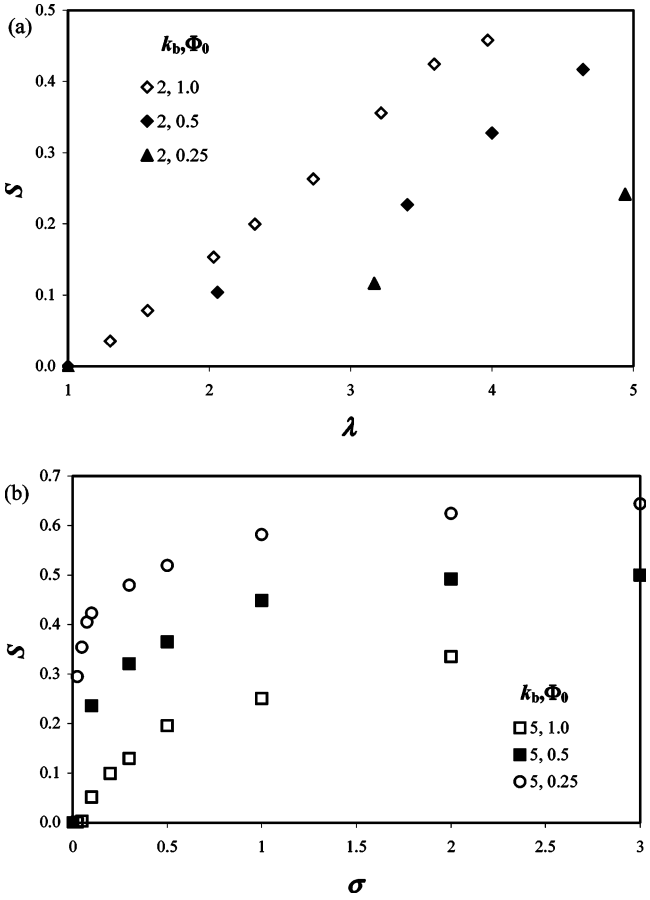

Figure 8. Segment order parameter S as a function of (a) λ for $k_b = 2$ and (b) σ for $k_b = 5$.

with a broader isotropic−nematic transition region. Cleary, a larger number of trapped entanglements will increase σ_{nem} since entanglements resist network deformation. Note also that trapped entanglements act uniformly throughout the system, are unlikely to completely *slip away* upon strain or ordering, and tend to lock in local disorder. This entanglement effect on σ_{nem} is consistent with the fact that a steeper (and potentially abrupt) change of S with stress is observed for a smaller Φ_0 (as in Figure 8b).

Figure 9 shows the segmental S values for all the bonds in an entangled network with $k_b = 2$ and $\Phi_0 = 1.0$. Also shown is the distribution expected for a random segment orientation (in which the fraction of segments corresponding to a particular angle θ with strain axis is proportional to sin θ). Expectedly, it is seen that the fraction of the most ordered segments increases with increasing stress. Note also that there is a significant fraction of nonoriented segments even at the highest stresses. It can be suggested that these disordered segments correspond to entangled regions along the chains that are restrained from aligning by their interactions with other chains. Figure 10 shows the distribution of the chain population according to their S values (averaged over the entire chains) for the same network (with $k_b = 2$ and $\Phi_0 = 1.0$). The data are sharply peaked at low stress, and the peak broadens with increasing stress. Upon stretching, a critical strain is reached beyond which a few chains become strongly aligned and severely limit further extension (resulting in an upturn in stress), while a large population of chains remains weakly aligned. For this system, the upturn occurs near $\sigma = 1$ (see Figure 6a) where a few

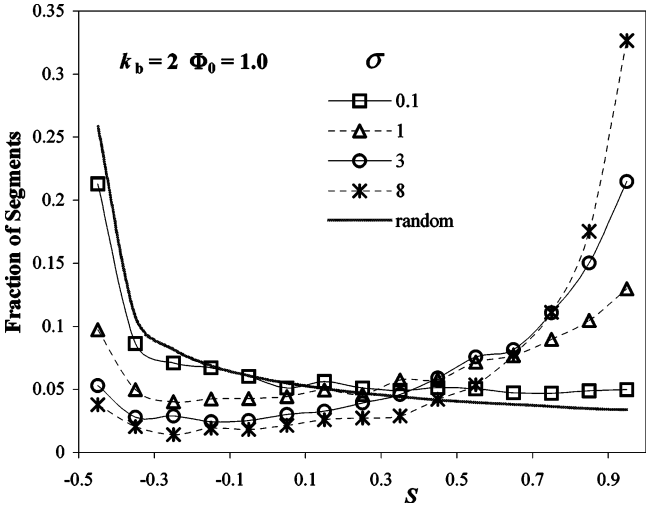

Figure 9. Histogram showing the distribution of segments according to their individual S values. The numbers representing various data series denote the stress applied on the sample; in all cases, $k_b = 2$ and $\Phi_0 = 1.0$. The "random" line is the distribution expected for randomly oriented segments.

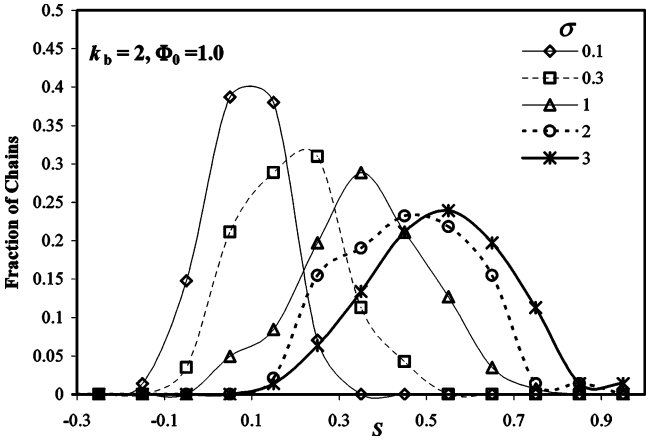

Figure 10. Histogram showing the distribution of chains according to the S values averaged over the chains. The numbers representing various data series denote the stress applied on the sample; in all cases, $k_b = 2$ and $\Phi_0 = 1.0$.

chains are seen to attain S values near 0.8 in Figure 10. This effect can also be seen in some system "snapshots" shown in Figure 11. Two stress values are considered: $\sigma = 2$ [$\lambda = 3.86$ − (a)] and $\sigma = 3$ [$\lambda = 4.31$ − (b), (c)]. Parts (a) and (b) show only those chains with chain order parameter values greater than 0.7, i.e., the most aligned chains. Part (c) depicts chains with chain order parameter values less than 0.35, i.e., the least oriented chains. It is seen that with increasing stress more and more chains are highly stretched and inhibit additional elongation of the sample. Note that the stretched chains in Figure 11b seem to span continuously (i.e., as if interconnected) the length of the simulation box, suggesting that they could be preferential stress carriers. It can also be seen that both the most and least oriented chains are more or less uniformly distributed throughout the system, though the least oriented chains seem to have less uniformity.

Our results also complement previous simulation studies of un-cross-linked semiflexible polymer melts.[34−37] The isotropic−nematic transitions that are observed in un-cross-linked systems (in the absence of strain) are made possible because the entanglements are not spatially trapped and can eventually redistribute and

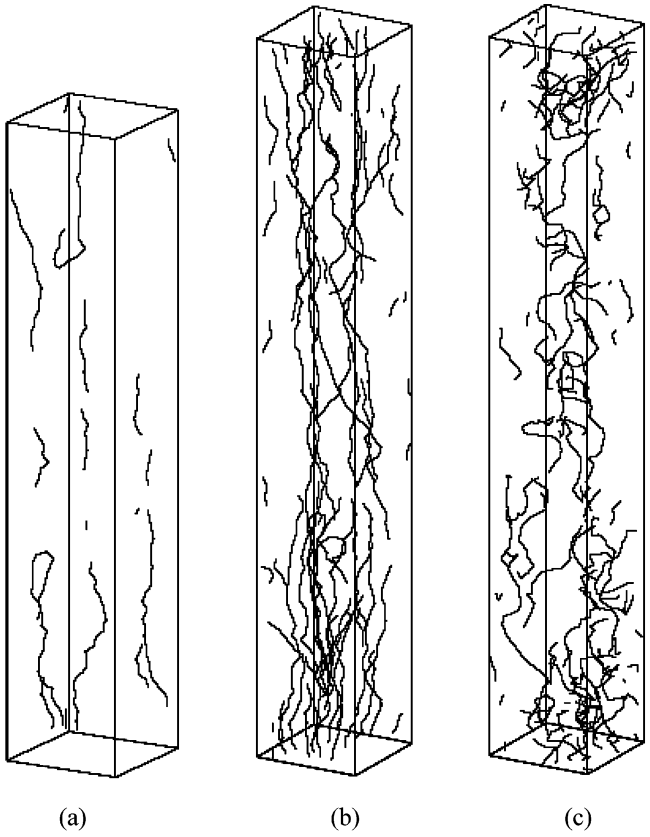

Figure 11. Selected snapshots of an entangled network ($k_b = 2$, $\Phi_0 = 1.0$) undergoing uniaxial extension. The leftmost image (a) is for $\sigma = 2$ and $\lambda = 3.86$. Images (b) and (c) correspond to $\sigma = 3$ and $\lambda = 4.31$. Images (a) and (b) only show chains whose chain order parameter is greater than 0.7. Image (c) shows only shows chains whose chain order parameter is less than 0.35. The apparent interruption in the conformations of chains near the box sides is due to the periodic boundaries.

even diminish. The theoretical predictions mentioned[27−29] previously—the appearance of an isotropic−nematic transition for stiff chain networks at high strains (∼500%)—do not consider entanglements. They also make the unreliable assumption of affine deformation. Naturally, these theoretical studies are not directly applicable to our entangled systems, which provide a more realistic description of end-linked chain networks. Mark et al.'s theoretical model[27−29] should, however, be well suited to describe the behavior of networks with little or no entanglements. As indicated earlier, our $\Phi_0 = 0.25$, $k_b = 5$ network from Figures 6b and 8b exhibited a fairly abrupt change of order with stress, and one could expect to observe a discontinuous order−disorder transition in our diamond networks. Such an expectation is confirmed by our preliminary results for 20-mer diamond networks shown in Figure 12 (using the modified potential cutoff described at the end of section 3.2). A first-order transition can be seen in the σ vs λ plot for $k_b = 5$ in the region where the strain changes discontinuously from $\lambda \approx 1.8$ to $\lambda \approx 3$ at an almost constant stress. In the S vs σ plot for $k_b = 5$, it is clear that S increases steeply before the transition and then remains almost constant at a nematic-like value of ∼0.57 (a behavior markedly different from that of the $k_b = 2$ network). It should be noted that even though an order−disorder transition is observed in these diamond networks, no theoretical predictions are available for equivalent systems to draw any direct comparison. (Our transition strain value is much lower than those

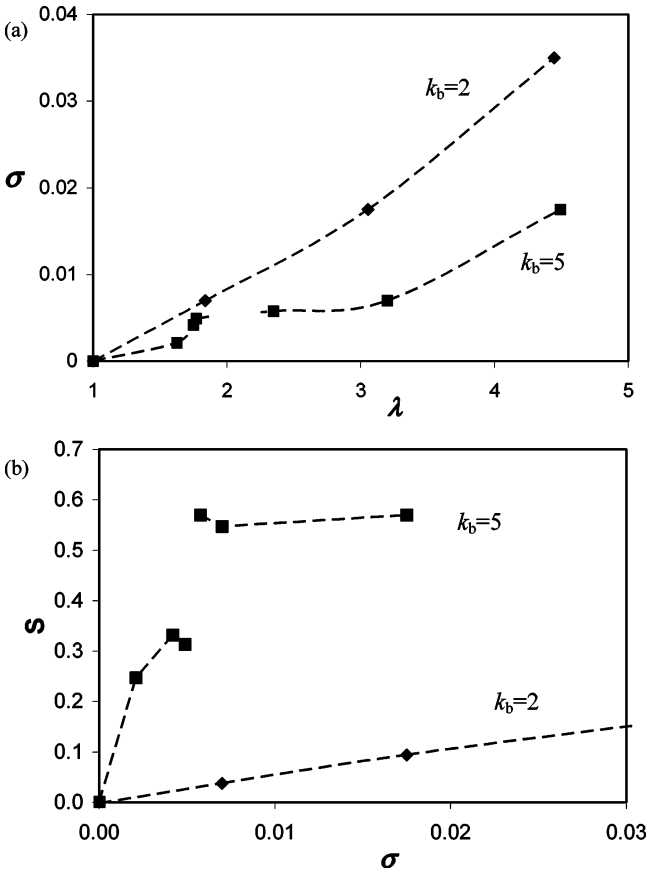

Figure 12. Stress (σ) vs λ data and segmental order (S) vs σ data for diamond networks with $r_c = 1.2\sigma_{LJ}$. Lines are drawn to guide the eye.

reported thus far.[27−29]) More detailed and extensive simulations for this kind of systems are currently underway.[51]

For our realistically entangled networks, we observe a gradual change from a random liquid phase to a nematic liquid crystalline phase upon stretching, where the density does not change appreciably. The absence of a semicrystalline mesomorphic state (that has a different density as compared to an amorphous melt) means that chain stiffness alone is not enough to explain the behavior of PDES elastomers. We expect that the use of energetic interactions that favor aligned packing of chains without contributing substantially to the entanglements will better capture the mesophasic behavior of PDES networks.

4. Conclusions

We have conducted the first reported simulation study on the effect of chain stiffness on the elastic properties of polymer networks. We have successfully adapted the simulation methods implemented by Chen et al.[25] to semiflexible chain polymer networks. The networks were prepared by equilibrating and end-linking a system of monodisperse 50-mer precursor chains on a lattice. The chain stiffness was controlled by the stiffness parameter k_b (=0, 2, and 5) through a bending potential. The extent of entanglements was controlled through the precursor volume fraction (Φ_0 = 1.0, 0.5, and 0.25). The resulting networks, having varying chain stiffness and degree of entanglements, were subjected to deformations using off-lattice isobaric and isostress ensemble simulations.

The extent of swelling was observed to decrease with increasing chain stiffness as a result of the corresponding increase of entanglements. Reducing the volume fraction at curing reduces the number of trapped entanglements which increases swelling. It was found that the exponent ζ in ($\Phi_{eq} \sim \Phi_0^{\zeta}$) is about 0.8 for both $k_b = 2$ and 5. This is close to the theoretical exponent describing entanglement dominated networks ($\zeta = 1.0$), reflecting the fact that semiflexible chain networks are closer to being entanglement dominated than their corresponding flexible chain networks (of equal length). The results from the diamond networks indicate that the stiffer chain networks actually would swell more if all the entanglements could be removed.

The shear modulus values for entangled networks, as determined from the Mooney−Rivlin plots, increase with chain stiffness. Semitheoretical estimates for the shear elastic modulus were obtained through the use of the RP[50] model for the fully flexible network and the simulation derived values of the entanglement molecular weight N_e.[39] It was found that these estimates agree well with the simulations for fully flexible chains ($k_b = 0$) and for moderately stiff chains ($k_b = 2$) but not for the very stiff chains ($k_b = 5$). Completely removing entanglements (as in diamond networks) causes stiffer chain networks to have a lower modulus as compared to flexible chains networks.

Order in the systems along the strain direction was calculated using the segmental order parameter S. It was found that increasing the degree of entanglements (via a larger Φ_0 or k_b) is associated with more order for systems at fixed strain, but with less order for systems at fixed stress. While entanglements foster ordering to some extent by causing the chains to interact more closely with each other, they also increase the amount of stress needed to attain a nematic-like ordering and thus broaden the order−disorder transition region. It is also found that some chain segments are too entangled to order and align even under very high stress. The origin of the observed sharp upturn in stress vs strain data lies in the fact that some chains become almost completely stretched beyond a critical strain and severely limit further extension of the entire network. Nearly athermal, entanglement-free diamond networks do show a first order order−disorder transition at very low stresses. Our results suggest that it should in principle be possible to prepare realistically end-linked networks from semiflexible chains (with $k_b \sim 5$ or larger) at low enough Φ_0 ($\Phi^* < \Phi_0 < 0.25$) to have so few trapped entanglements to approach the behavior of diamond networks and exhibit a discontinuous strain-induced ordering transition. Work along this direction is currently under way.

Our entangled network systems do not exhibit the strain-induced ordering transition observed in PDES elastomers, and therefore, chain stiffness alone is not sufficient to describe the behavior of PDES. Our future efforts on this issue are directed toward using an interchain potential that promotes alignment between chains.

Acknowledgment. This work was supported by the Polymers Program of the National Science Foundation, Grants DMR-0078863 and 0349952. The authors are grateful to N. Gilra and Prof. A. Z. Panagiotopoulos for an early version of the BFM code, to Z. Chen for help

with some simulation details, and to A. Batra and Prof. T. M. Duncan for valuable comments.

References and Notes

(1) Flory, P. J.; Rehner, J. *J. Chem. Phys.* **1943**, *11*, 512.
(2) Wall, F. T. *J. Chem. Phys.* **1943**, *11*, 527.
(3) James, H. M.; Guth, E. *J. Chem. Phys.* **1943**, *11*, 455.
(4) James, H. M.; Guth, E. *J. Chem. Phys.* **1947**, *15*, 669.
(5) Treloar, L. R. G. *The Physics of Rubber Elasticity*; Clarendon Press: Oxford, England, 1958.
(6) Ronca, G.; Allegra, G. *J. Chem. Phys.* **1975**, *63*, 4990.
(7) Flory, P. J. *J. Chem. Phys.* **1977**, *66*, 5720.
(8) Erman, B.; Flory, P. J. *J. Chem. Phys.* **1978**, *68*, 5363.
(9) Flory, P. J.; Erman, B. *Macromolecules* **1982**, *15*, 800.
(10) Edwards, S. F. *Proc. Phys. Soc.* **1967**, *92*, 9.
(11) Edwards, S. F. *Br. Polym. J.* **1977**, *9*, 140.
(12) Eichinger, B. E. *Annu. Rev. Phys. Chem.* **1983**, *34*, 359.
(13) Heinrich, G. *Adv. Polym. Sci.* **1988**, *85*, 33.
(14) Edwards, S. F.; Vilgis, T. A. *Rep. Prog. Phys.* **1988**, *51*, 243.
(15) Duering, E. R.; Kremer, K.; Grest, G. S. *Phys. Rev. Lett.* **1991**, *67*, 3531.
(16) Duering, E. R.; Kremer, K.; Grest, G. S. *J. Chem. Phys.* **1994**, *101*, 8169.
(17) Everaers, R.; Kremer, K. *Macromolecules* **1995**, *28*, 7291.
(18) Everaers, R.; Kremer, K. *Phys. Rev. E* **1996**, *53*, R37.
(19) Kenkare, N.; Smith, S. W.; Hall, C. K.; Khan, S. A. *Macromolecules* **1998**, *31*, 5861.
(20) Hölzl, T.; Trautenberg, H. L.; Göritz, D. *Phys. Rev. Lett.* **1997**, *79*, 2293.
(21) Everaers, R. *New J. Phys.* **1999**, *1*, 12.1−12.54.
(22) Escobedo, F. A.; de Pablo, J. J. *J. Chem. Phys.* **1996**, *104*, 4788.
(23) Escobedo, F. A.; de Pablo, J. J. *J. Chem. Phys.* **1997**, *106*, 793.
(24) Kenkare, R.; Hall, C. K.; Khan, S. A. *J. Chem. Phys.* **2000**, *113*, 404.
(25) Chen, Z.; Cohen, C.; Escobedo, F. A. *Macromolecules* **2002**, *35*, 3296.
(26) Godovsky, Yu. K. *Angew. Makromol. Chem.* **1992**, *202*, 187.
(27) Erman, B.; Bahar, I.; Kloczkowski, A.; Mark, J. E. *Macromolecules* **1990**, *23*, 5335.
(28) Bahar, I.; Erman, B.; Kloczkowski, A.; Mark, J. E. *Macromolecules* **1990**, *23*, 5341.
(29) Yong, Y.; Kloczkowski, A.; Mark, J. E.; Erman, B.; Bahar, I. *Macromolecules* **1995**, *28*, 4920.
(30) Warner, M.; Terentjev, E. M. *Prog. Polym. Sci.* **1996**, *21*, 853.
(31) Warner, M.; Terentjev, E. M. *Liquid Crystal Elastomers*; Oxford University Press: New York, 2003.
(32) Hedden, R. C.; Saxena, H.; Cohen, C. *Macromolecules* **2000**, *33*, 8676.
(33) Kaufhold, W.; Finkelmann, H.; Brand, H. R. *Makromol. Chem.* **1991**, *192*, 2555.
(34) Wilson, M. R.; Allen, M. P. *Mol. Phys.* **1993**, *80*, 277.
(35) Dijkstra, M.; Frenkel, D. *Phys. Rev. E* **1995**, *51*, 5891.
(36) Escobedo, F. A.; de Pablo, J. J. *J. Chem. Phys.* **1997**, *106*, 9858.
(37) Yethiraj, A.; Fynewever, H. *Mol. Phys.* **1998**, *93*, 693.
(38) Shibanov, Y. D. *Polym. Sci. U.S.S.R.* **1989**, *31*, 2653.
(39) Faller, R.; Müller-Plathe, F. *ChemPhysChem* **2001**, *2*, 180.
(40) Kavassalis, T. A.; Noolandi, J. *Macromolecules* **1989**, *22*, 2709.
(41) Deutsch, H.-P.; Binder, K. *J. Chem. Phys.* **1991**, *94*, 2294.
(42) Paul, W.; Binder, K.; Heermann, D.; Kremer, K. *J. Phys. II* **1991**, *1*, 37.
(43) Gilra, N.; Cohen, C.; Panagiotopoulos, A. Z. *J. Chem. Phys.* **2000**, *112*, 6910.
(44) Fynewever, H.; Yethiraj, A. *J. Chem. Phys.* **1998**, *108*, 1636.
(45) Allen, M. P.; Tildesley, D. J. C*omputer Simulation of Liquids*; Clarendon: Oxford, 1987.
(46) Obukhov, S. P.; Rubinstein, M.; Colby, R. H. *Macromolecules* **1994**, *27*, 3191.
(47) Pütz, M.; Kremer, K.; Grest, G. S. *Europhys. Lett.* **2000**, *49*, 735.
(48) Roland, C. M.; Mott, P. H. *Macromolecules* **1998**, *31*, 4033.
(49) Graessley, W. W. *Polymeric Liquids and Networks*; Taylor and Francis: New York, 2003.
(50) Rubinstein, M.; Panyukov, S. *Macromolecules* **1997**, *30*, 8036.
(51) Bhawe, D. M.; Cohen, C.; Escobedo, F. A. Manuscript in preparation.

MA0354896